PERGAMON

Atmospheric Environment 35 (2001) 4315–4330

ATMOSPHERIC ENVIRONMENT

www.elsevier.com/locate/atmosenv

Estimating PM_{10} air concentrations from dust storms in Iraq, Kuwait and Saudi Arabia

Roland R. Draxler[a,*], Dale A. Gillette[b], Jeffrey S. Kirkpatrick[c], Jack Heller[c]

[a] *NOAA, Air Resources Laboratory (R/ARL), 1315 East West Highway, Silver Spring, MD 20910, USA*
[b] *NOAA, Atmospheric Sciences Modeling Division (MD-81), Research Triangle Park, NC 27711, USA*
[c] *US Army Center for Health Promotion and Preventive Medicine, 5158 Blackhawk Road, Aberdeen Proving Ground, MD 21010, USA*

Received 1 September 2000; accepted 11 February 2001

Abstract

A model for the emission of PM_{10} dust has been constructed using the concept of a threshold friction velocity which is dependent on surface roughness. Surface roughness in turn was correlated with geomorphology or soil properties for Kuwait, Iraq, part of Syria, Saudi Arabia, the United Arab Emirates and Oman. The PM_{10} emission algorithm was incorporated into a Lagrangian transport and dispersion model. PM_{10} air concentrations were computed from August 1990 through August 1991. The model predicted about the right number of dust events over Kuwait (events occur 18% of the time). The model results agreed quantitatively with measurements at four locations in Saudi Arabia and one in Kuwait for one major dust event ($>1000\,\mu g/m^3$). However, for smaller scale dust events (200–$1000\,\mu g/m^3$), especially at the coastal sampling locations, the model substantially over-predicted the air concentrations. Part of the over-prediction was attributed to the entrainment of dust-free air by the sea breeze, a flow feature not represented by the large-scale gridded meteorological data fields used in the model computation. Another part of the over-prediction was the model's strong sensitivity to threshold friction velocity and the surface soil texture coefficient (the soil emission factor), and the difficulty in accurately representing these parameters in the model. A comparison of the model predicted PM_{10} spatial pattern with the TOMS satellite aerosol index (AI) yielded a spatial pattern covering a major portion of Saudi Arabia that was quite similar to the observed AI pattern. Published by Elsevier Science Ltd.

Keywords: Long-range transport; Southwest Asia; Resuspension; Aeolian movement; HYSPLIT

1. Introduction

Large scale emissions and transport of fine particulate matter from dust storms, especially from the Sahara, has been extensively studied and compared with satellite observations and other remote probing methods (Karyampudi et al., 1999; Westphal et al., 1987). We adapted a method used to predict dust injections from the Sahara desert (Marticorena and Bergametti, 1995) to dust emissions over southwestern Asia (Iraq, Kuwait, and Saudi Arabia). The mass source algorithm for PM_{10} (particles with a diameter of $10\,\mu m$ or less) is used as a component in a regional transport and dispersion model to compute ground-level air concentrations of PM_{10}. The air concentration data are to be used for health assessments in the area occupied by US troops during the Gulf War period (August 1990 through April 1991) prior to the onset of surface-based sampling. Data needed to implement the algorithm are the threshold friction velocities for initiation of dust emission, the aerodynamic roughness length of the surface, and a coefficient that relates surface soil texture to PM_{10} dust emissions. These parameters were

*Corresponding author.
E-mail address: roland.draxler@noaa.gov (R.R. Draxler).

1352-2310/01/$ - see front matter Published by Elsevier Science Ltd.
PII: S1352-2310(01)00159-5

Nomenclature

A	areal of the emission cell
C_D	drag coefficient
C_{Dns}	drag coefficient for non-saltating conditions
C_{Ds}	drag coefficient for saltating conditions ($U > U_t$)
D_p	mean soil particle diameter
f_{eff}	the efficient friction velocity ratio
F	vertical mass flux of PM_{10} dust
g	acceleration due to gravity.
k	von Karman's constant
K	surface soil texture coefficient
M	the pollutant mass assigned to a particle
P	fraction of the cell covered by a single soil roughness class
P	three-dimensional particle position vector
ρ	air density
Q_{tot}	total aeolian horizontal mass flux
R	the particle number emission rate per grid cell per time step
σ	internal dispersion model terrain following vertical coordinate
u_*	friction velocity
u_{*s}	friction velocity for a smooth surface
u_{*ts}	threshold friction velocity for a smooth surface
U_{*t}	threshold friction velocity for initiation of dust emission
U	wind speed
U_t	threshold wind speed
W	three dimensional velocity vector
Z	wind measurement height
Z_{0S}	roughness length of the soil without any roughness elements
Z_{0NS}	aerodynamic roughness length for non-saltating ($U \leqslant U_t$) conditions
Z_{top}	top of the Hysplit coordinate system
Z_{sfc}	the height of the ground
Z_{msl}	vertical coordinate height above sea-level.

estimated using a "bootstrap" method that started with small-scale data on soil characteristics, estimation of soil size distribution, and then relating the threshold friction velocity to the aerodynamic roughness length of the surface. Using maps of larger-scale soil features, these local parameters were extended to estimate the dust emission potential over the whole domain.

A dust emission rate was computed from each cell when the local wind velocity exceeded the threshold velocity for the soil characteristics of that emission cell. The dominant mechanism for the PM_{10} dust input model is "sand-blasting". The emitted material was dispersed and transported using a modified Lagrangian particle-puff model (Draxler and Hess, 1998) using gridded meteorological data fields. Computations were made for the period of August 1990 through August 1991. During this time there was extensive soil disturbance in the region due to military maneuvers that culminated in the Gulf War during January and February of 1991. Ground-based PM_{10} sampling was started in May of 1991. The model calculated air concentrations from mid-May through mid-July, the period of the most frequent and intense dust storms. These calculations were compared with the measured data. Spatial patterns of the model predictions were also compared with the aerosol index parameter derived from the TOMS satellite instrument.

2. PM_{10} source algorithm

2.1. Emission flux

The mass source algorithm of Marticorena et al. (1997) is used to compute PM_{10} dust injections, where the vertical mass flux of dust,

$$F = K\frac{\rho}{g}u_*(u_*^2 - u_{*t}^2), \tag{1}$$

is calculated from the friction velocity (u_*), a threshold friction velocity (u_{*t}) required for initiation of dust emission, and a coefficient (K with units m^{-1}) that relates the surface soil texture to PM_{10} dust emissions. Following conventional notation, ρ is air density and g is the acceleration of gravity. The friction velocity may vary in space and time because it depends upon both the local meteorological conditions and the surface roughness. However, the threshold velocity and soil texture coefficient vary only in space and can be related to the surface roughness, soil, and land-use characteristics.

2.2. Local friction velocity

Given a value of u_{*t} one can calculate the threshold wind speed

$$U_t = \frac{u_{*t}}{k}\ln\left(\frac{z}{z_{0NS}}\right), \tag{2}$$

where z_{0NS} is the aerodynamic roughness length for non-saltating ($U \leqslant U_t$) conditions, z is the wind measurement height, and Von Karman's constant (k) is assumed to equal to 0.4. The drag coefficient C_{Dns} for non-saltating conditions is

$$\sqrt{C_{Dns}} = \frac{k}{\ln(z/z_{0NS})} \tag{3}$$

and the drag coefficient C_{Ds} for saltating conditions ($U > U_t$; Gillette et al., 1998) is

$$\sqrt{C_{Ds}} = \sqrt{C_{Dns}} + 0.003\left(1 - \frac{U_t}{U}\right). \tag{4}$$

Then for $U < U_t$, $C_D = C_{Dns}$ and for $U > U_t$, $C_D = C_{Ds}$ and

$$u_* = \sqrt{C_D}U, \tag{5}$$

where U is the wind speed. Computationally each potential emission location has a predefined u_{*t}, z_{0NS}, and K (the coefficient for PM_{10} emission from Eq. (1). PM_{10} is only emitted from that location when $U > U_t$. Determination of these three constants for southwest Asia is described in the following sections.

2.3. Threshold friction velocity

There is a hierarchy of mechanisms controlling u_{*t}. First, for loose or disturbed soils, the most important parameter is roughness of the surface. The roughness (including vegetation) acts to absorb part of the momentum of the wind. Second, the soil size distribution has an effect for loose soils if there is a lack of particles that correspond to the minimum threshold. Third, soil crusting affects threshold friction velocity. Crusted soils, whether biological (cyanobacterial lichen soil crusts—CLC) or physically formed, resist wind erosion. If a crust is partially broken, the size of erodible units is important along with the roughness. In general CLC crusts are more protective crusts since the biological fibrous growth roughens the surface and aggregates soil particles even after the crust is dry and even when the biological material is dead. In summary, only undisturbed loose soils and disturbed soils of all types would be expected to be erodible under normal wind conditions.

Patterns of disturbance by both animals and humans are of primary importance in making predictions of wind erosion. El-Baz (1994) extensively reviewed the disturbance to the desert surface of Kuwait during the Gulf War. He estimated that 30.6% of the total surface area of Kuwait was impacted by war related activities. By far, the largest area of disturbance was caused by the explosion, search, and removal of mines. The effect of a disturbance is to lower the threshold for wind erosion (Gillette, 1983). This is caused by burying of gravel-size surface particles, breakage of crust, and destruction of vegetation. Vegetation also is a protector of the soil from wind erosion. However, vegetation is extremely limited on the desert landscapes that are probable dust source areas and therefore will not be considered. Likewise, crusted soils are probably not dust sources.

We used the method of Marticorena and Bergametti (1995) to calculate threshold friction velocity u_{*t} for unvegetated, uncrusted soils from knowledge of surface roughness and size distribution of loose particles on the surface. The calculation of the threshold friction velocity is given as

$$u_{*t}(D_p, z_0) = \frac{u_{*ts}(D_p)}{f_{eff}}, \tag{6}$$

where u_{*ts} is the threshold friction velocity for a smooth surface, D_p is the mean soil particle diameter, and f_{eff} is the efficient friction velocity ratio. f_{eff} is defined by Marticorena and Bergametti (1995) as the ratio of local to total friction velocity

$$f_{eff} = \frac{u_{*s}}{u_*} = 1 - \left[\frac{\ln[z_0/z_{0s}]}{\ln[0.4[10/z_{0s}]}\right]. \tag{7}$$

The roughness length of the soil z_{0S} without any roughness elements was estimated by Greeley and Iversen (1985) to be $z_{0S} = D_p/30$. For the size range of particles most easily mobilized (88–125 μm; Greeley and Iversen, 1985), this relation provides roughness lengths ranging from 3×10^{-4} to 4×10^{-4} cm. Such values are consistent with measurements made in wind tunnels for smooth, loose soils (Gillette et al., 1982; McKenna-Neuman and Nickling, 1994; Li and Martz, 1994). Values for $u_{*ts}(D_p)$ may be calculated from the expressions given by Iversen and White (1982). The threshold friction velocity of the smooth, loose soil as a whole is the same as the threshold friction velocity of the loose surface particles of size D_p that have the minimum $u_{*ts}(D_p)$.

A collection of 38 soil samples were analyzed for size distribution. The samples were collected at various locations in Kuwait, Saudi Arabia, and Iraq in 1991, 1994, and 1996. The samples were processed for size distribution of the dry aggregated soil material without physical or chemical alteration. Size distributions were done on the composite samples of the individual grains making up the aggregated soil material. The samples were processed by the University of Colorado Institute for Arctic and Alpine Research Sediment Laboratory. The sediments were passed through a 2000 μm screen without de-aggregation procedures.

The size distributions results showed that every sample had an abundance of at least 2.5% and mean of 9.2% by mass in the particle size range 88–125 μm. Using a mean value of u_{*t} of 22 cm/s in Eq. (6) corresponding to the size range 88–125 μm, and $z_{0S} = 4.1 \times 10^{-4}$ cm (one-thirtieth of the largest diameter

of this optimal size range) in Eq. (7), we estimated u_{*t} for a range z_0 expected in the dust source areas. Supplemental data on size distributions from Iraq (Skocek and Saadallah, 1972) showed that from 10% to 30% of "traveling sands" had mass with particles between 63 and 125 μm. Binda (1983) showed that dune sands in Saudi Arabia have a fraction of mass in particles between 63 and 125 μm. Our size distributions along with those of Skocek and Saadallah and Binda show that particles of size 88–125 μm are almost omnipresent in the southwest Asia desert surface sediments.

2.4. Estimation of local aerodynamic roughness heights for Southwest Asia

From the arguments developed in Section 2.2, we assert that the variations of the threshold wind friction velocity for loose and undisturbed soil are controlled by the changes in the surface roughness. Further, experience in the United States showed that dust emissions are dominated by loose, uncrusted soils and disturbed soils (Gillette, 1983). The results of the application of the above model depend on the accurate assignment of roughness lengths for non-saltating conditions and soil conditions (loose or crusted) over the model domain.

Studies of threshold friction velocities done in the Mojave desert in the western United States were carried out by Gillette et al. (1980, 1982). A portable wind tunnel was used to develop the neutral wind profiles over the natural desert surfaces. Aerodynamic roughness heights were obtained by extrapolation using the detailed profiles near the surface. Gillette (1983) pointed out that threshold friction velocities correlate with desert geomorphology for the Mojave desert. We used the conceptual framework that aerodynamic roughness length will control the threshold friction velocity for a desert where particles of the size 88–125 μm are always available. Further, z_0 may be mapped because of a correlation with geomorphic or soil-mapping classification.

Assignment of typical z_0 values to surficial features was done for Kuwait by using remote sensing imagery of the surface along with a map of surficial features. For Iraq and the rest of the Arabian Peninsula, the Kuwaiti surface classes were related to the mapping classifications used by the appropriate regional soil and geomorphology maps. The detailed soil mapping of Buringh (1960) was used for Iraq. Areas to the east of the Euphrates River (with the exception of desiccated flood plain soils at the confluence of the Tigris and Euphrates Rivers) were not considered because of vegetative cover or agricultural soils. A map showing the most active aeolian deposits (Stevens, 1978) and a revision of the US Geological Survey map (United Kingdom Series edition 5211 2-GSGS) of the Arabian Peninsula was used to identify surface types and geomorphology in Saudi Arabia.

A remote sensing mosaic image of the Kuwait surface is shown in Fig. 1. It shows features such as bright areas, sinuous curves identified as sand dunes, and darker areas near the shoreline of the Arabian Gulf. Some features such as airports help locate most of the points on the mosaic. The presence of streaks in Fig. 1 in the west-central part of the figure is a feature typical of aeolian activity. The fact that the streaks line up with the dominant high wind direction is a confirmation that active wind erosion has taken place. These streaks are seen with dune-like structures. These dunes are geomorphological features correlating with active sand movement.

A map of surface conditions and geomorphology of Kuwait by Gharib et al. (1985) was compared to Fig 1. Many homogeneous-appearing areas of Fig. 1 can be identified by a single independent surficial unit. Using the Gharib's geomorphological classifications and our z_{0NS} data coupled with u_{*t} data from the Mojave desert (Gillette et al., 1980, 1982) we estimated typical u_{*t} and z_0 values for each surface classification. Because several of these classifications were found to possess the same u_{*t} and z_0 values, we defined seven classes incorporating groups of Gharib et al.'s classifications. These classes and parameters are given in Table 1. For example, an area in the southeast part of Fig. 1 show sinuous structures that may be associated with barchanoid dunes. Their mottled color—green mixed with brown in the original mosaic—suggests that they are vegetated and consequently have a relatively high threshold friction velocity. This area is set in class 4. In the northwestern part of the area covered in Fig. 1, a similar structure suggests dunes, but lack of green color also suggests that the dunes are not stabilized. This probably is a dust producing area, classified as an "active sand sheet" (class 3). The area in the southwest part of the land represented in Fig. 1 has a bright appearance. This appearance is likely produced by high albedo smooth, un-vegetated sand and was also classified as an active sand sheet. The area also has streaks that align with the dominant high wind. These streaks provide corroborating evidence for aeolian movement. Areas near the Arabian Gulf, classified as "urban areas" and "coastal plain deposits" (class 5), have low brightness and correspond to vegetation and built-up areas having non-dust producing rough surfaces. Finally, the area in southwestern Kuwait classified as "covered desert floor" (class 7), has a pebbly granule lag surface and is less bright in appearance in Fig. 1. This rough surface is not as bright as a smooth sandy surface because the reflection is diffused. The classification scheme of Table 1 was extended to Iraq using soil maps (Buringh, 1960), and to Saudi Arabia and other countries south of

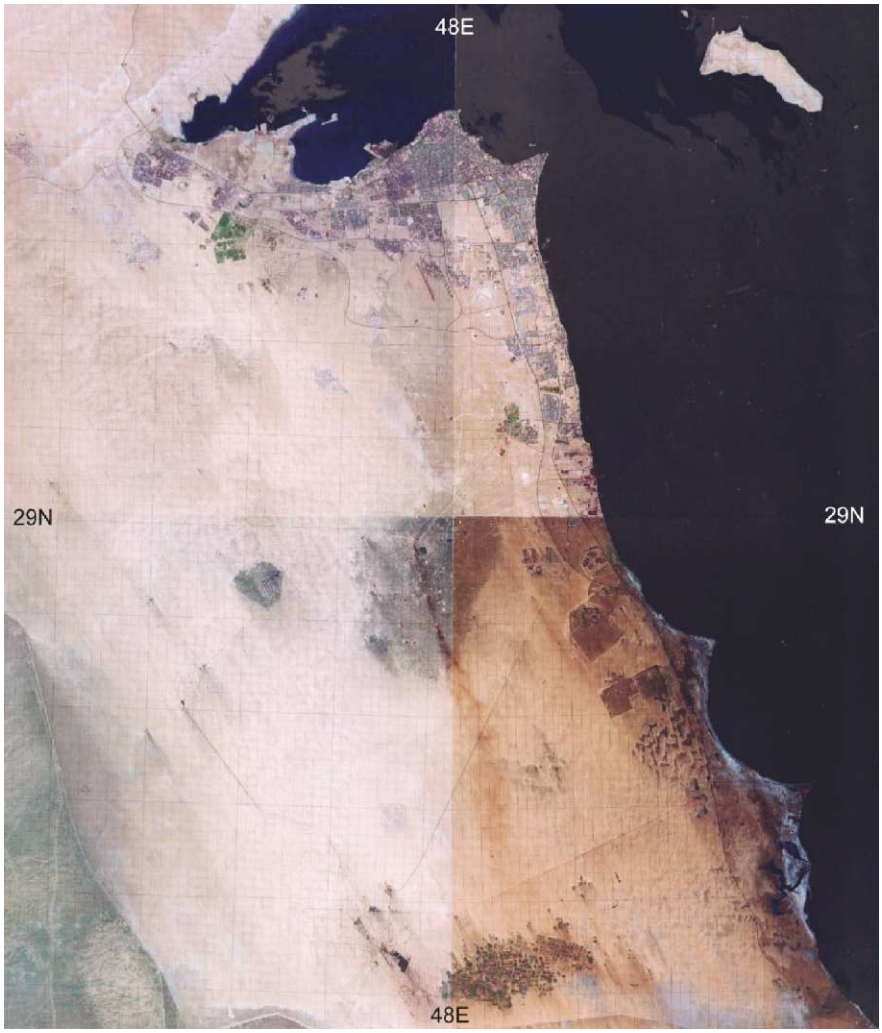

Fig. 1. Aerial remote sensing mosaic of eastern Kuwait from NOAA's AVHRR showing a 1° square of latitude–longitude centered about 29°N and 48°E as indicated by the light lines crossing through the center of the illustration.

Table 1
Roughness classes using Gharib et al.'s (1985) surficial classifications with their assigned roughness length and threshold friction velocity

Class	Roughness identification	z_{0S} (m)	u_{*t} (m/s)
1	Gravel Lag	2×10^{-4}	1.0
2	Deflated Sand Sheet	4×10^{-4}	0.62
3	Active Sand Sheet	2×10^{-5}	0.28
4	Smooth Sand Sheet	5×10^{-4}	0.69
5	Coastal Plain Deposits	3×10^{-3}	3.5
6	Playa Deposits	2×10^{-5}	3.0
7	Covered Desert Floor	2×10^{-4}	0.75

Kuwait in the Arabian penninsula using geomorphology maps (United Kingdom Series edition 5211 2-GSGS, 1980).

2.5. Surface soil texture parameter

The parameter K of Eq. (1) is derived from the ratio of vertical flux of PM_{10} (F) to total aeolian horizontal mass flux (Q_{tot}). Fig. 2 shows the ratio for several soils of semi arid and arid areas of the United States presented by Gillette et al. (1997). The vertical flux F of particles smaller than 10 μm was estimated from their vertical profile. The horizontal flux Q_{tot} was measured using a Bagnold catcher. The illustration shows that the F/Q_{tot} results are widely scattered, but for the "sand" and texture the ratio lies within a range of 2×10^{-5}–1×10^{-3} 1/m. Values are lower for samples from "clay" soil textures and higher for loamy sand. The single value having a "loam" texture lies in the range occupied by the "sand" textures. The probable cause for the range of the F/Q_{tot} values for "sand" textures is similarity in size for

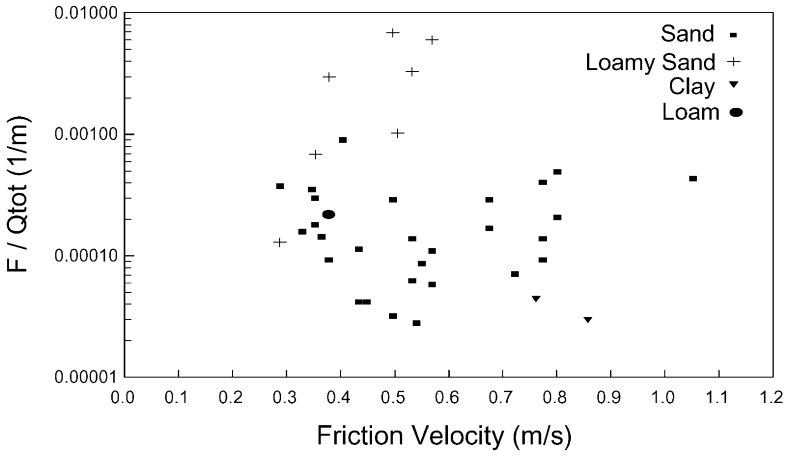

Fig. 2. The ratio of the vertical flux of PM_{10} to horizontal flux of total particle mass versus friction velocity for different soil textures (after Gillette et al., 1997).

saltating particles and similar binding energies for the sampled "sand" soils.

The percentage of sand was no less than 87.5% for 94% of the surface soil samples in the present study. This means that all these samples have "sand" textures or are at most 2.5% sand composition away from the "sand" texture. The overwhelming majority of samples imply a "sand" surface texture. Gillette et al. (1997) found that F/Q_{tot} for sand textured soils was 2×10^{-4} 1/m, which gives a K value for Eq. (1) of 5.6×10^{-4} 1/m. This follows from the ratio found for Q_{tot} to $(\rho/g)\, u_*(u_*^2 - u_{*\mathrm{t}}^2)$ of 2.8 (Gillette et al., 1996).

3. Transport and dispersion model

3.1. Overview

The Hybrid single-particle lagrangian integrated trajectory) (Hysplit_4) model is a complete system for computing simple trajectories to complex dispersion and deposition simulations using either puff or particle approaches. A complete discussion of an earlier version of the model is given in Draxler (1992). The updated advection algorithms of HYSPLIT_4 are described in Draxler (1996) and the entire modeling system and verification examples are presented in Draxler and Hess (1998).

The model calculation method is a hybrid between Eulerian and Lagrangian approaches. Advection and diffusion calculations are made in a Lagrangian framework while concentrations are calculated on a fixed grid. The transport and dispersion of a pollutant is calculated by assuming the release of a single puff or from the dispersal of a cluster of particles. A single released puff will expand until its size exceeds the meteorological grid cell spacing and then it will split into several puffs. An alternate approach, following Hurley (1994), is to combine both puff and particle methods by assuming a puff distribution in the horizontal and particle dispersion in the vertical direction. In this way, the greater accuracy of the vertical dispersion of the particle model is combined with the advantage of having an expanding number of puffs represent the pollutant horizontal distribution. Air concentrations are calculated at a specific grid point for puffs and as cell-average concentrations for particles. A concentration grid is defined by latitude–longitude intersections. A complete and detailed description of the model is available by Draxler and Hess (1997). However, a summary of the changes required to integrate the dust algorithm into the model's emission module is described in the following sections.

3.2. Advection and dispersion computation

In this fully three-dimensional model, calculations are performed with temporally varying gridded meteorological data using archived fields. Pollutant particles or puffs are transported through the domain and the dispersion is calculated along the trajectory. The trajectory of a particle or puff, or the change of its position vector ($\mathbf{P}$) with time,

$$\mathbf{P}(t + \Delta t) = \mathbf{P}(t) + 0.5[\mathbf{W}(\mathbf{P}, t) + \mathbf{W}(\{\mathbf{P}(t) + \mathbf{W}(\mathbf{P}, t)\Delta t\}, \mathrm{t} + \Delta t)]\Delta t, \quad (8)$$

is computed from the average of the three–dimensional velocity vectors ($\mathbf{W}$) at their initial and first-guess positions. Particle dispersion is computed by adding an

additional velocity term to the advection Eq. (8) that includes a contribution from a turbulent velocity component,

$$W'(t+\Delta t) = R(\Delta t)W'(t) + W''(1 - R(\Delta t)^2)^{0.5}, \quad (9)$$

which depends upon the turbulent velocity component at the previous time $W'(t)$, a velocity auto-correlation coefficient (R), and a computer-generated random component (W''). The vertical turbulent velocity component is computed from the diffusivity profile which is a function of the profiles of wind and temperature and the mixed-layer depth. The mixed-layer depth is estimated to be the height at which the potential temperature exceeds the surface value by 2°. Puff dispersion calculations are made by computing their rate of growth based upon the same turbulent velocity component used for particle dispersion. Air concentrations are computed by averaging the contribution from all puffs that pass over the grid node or for particles by computing the average particle mass divided by the cell volume.

Most Lagrangian models treat emissions as a point source. However the dust emissions occur over a larger area. In this situation the puff-particles are released from each emission cell, each advection time step, with an initial horizontal puff radius that is adjusted so that the horizontal puff area equals the area (A) of the emission cell. The initial pollutant mass is given by

$$M = R^{-1} \sum_{i=1}^{7} (F_i A P_i), \quad (10)$$

where F is from Eq. (1), P is the fraction of the cell covered by soil roughness class i, and R is the particle number emission rate (one particle per grid cell per time step). Particles are only emitted when the wind speed at that time and location exceeds the threshold speed for that class.

3.3. Meteorological data

Gridded meteorological analysis data from the European Centre for Medium Range Weather Forecasting (ECMWF, 1995) were used for the computational period of August 1990 through August 1991. The data files were obtained in a special format, on multiple files and tapes, by synoptic time, surface, upper air, and supplemental variables, all at a spatial resolution of 1.125° every 6 h. In the vertical the data were provided at 31 levels on the native ECMWF hybrid grid. These data were then interpolated to a Lambert Conformal grid at 60 km resolution, one file per month, with records in each file organized by time and height to permit simple access methods during the transport and dispersion computations. Wind components are defined relative to the grid orientation. The final computational grid of 65×65 points was centered at 30°N 45°E, covering the entire region from 12°N–28°E to 45°N–69°E. For clarity only an extract of the modeling domain (centered over Kuwait) is shown in Fig. 3. The map shows the location of the meteorological grid points and the PM_{10} sampling locations, to be discussed in more detail in the following section.

The computational meteorological file was at the same vertical resolution as the original data but only contained the first 20 levels from the ground (including 2 m temperature and 10 m winds) to about 200 hPa. Resolution is fairly good with six levels at or below 1500 m above ground level (about 40, 170, 410, 710, 1060, and 1460 m agl). The Hysplit code linearly interpolates the meteorological data from the ECMWF coordinate system to an internal model terrain following (σ) coordinate system

$$\sigma = (Z_{top} - Z_{msl})/(Z_{top} - Z_{sfc}), \quad (11)$$

where Z_{top} is the top of the Hysplit coordinate system — set to 25 km for these calculations, Z_{sfc} is the height of the ground, and Z_{msl} is the level's height above sea-level. The internal computational grid structure was defined for 18 levels, with the first few at 10, 75, 200, 385, 630, 935, 1300,... up to 10,000 m agl. The meteorological data are used in both the advection and dispersion calculations and full reflection is assumed for all particles that reach the top or bottom boundaries, but particles intersecting the ground surface lose a fraction of their mass through gravitational settling based upon the ratio of the settling velocity to the depth of the surface layer.

3.4. Integration of PM_{10} source algorithm

As discussed in Section 2.4, the roughness characteristics identified in Table 1 were identified on each

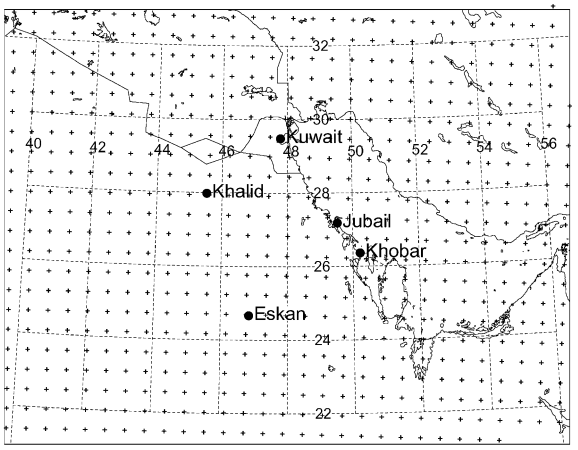

Fig. 3. Extract of Hysplit modeling domain showing the locations of the meteorological grid points (+) and the PM_{10} air concentration sampling stations.

regional map and the resulting source area information was organized by defining up to 3 of the 7 "roughness categories" of Table 1 per square of land (emission grid cell) and the percent of that square covered by each of the three (or fewer) categories. The sum of the percentages of the three categories may not add up to 100; the remaining percentage is assumed not to emit dust. For each square, the center point latitude and longitude was identified along with the length of the sides of the square which were either 0.5°, 1°, or 2° squares. Taken together, the boxes define a roughness class and threshold friction velocity for all the area in Kuwait, Iraq, part of Syria, Saudi Arabia, the United Arab Emirates and Oman. Areas outside of the defined area are assumed to not emit PM_{10} dust. To account for the fact that up to 30% (Section 2.3) of Kuwait's surface area was disturbed by activities related to the Gulf War and because it was impossible to quantify the disturbance in each cell, all emission squares were defined to have at least 10% of their area associated with Class 3 if not already defined as Class 3. Disturbed soils behave like Class 3 soils (Gillette et al., 1982). The manual classification method could only resolve soil types at roughly 5% areal increments and therefore 10% was the minimum value above the classification threshold.

For computational purposes all of the larger squares were sub-divided into 0.5° squares with the same roughness class to maintain a greater degree of consistency between the emission areas and resolution of the meteorological data. An examination of Table 1 shows that the lowest threshold friction velocity (0.28 m/s) is associated with Class 3 and the next higher friction threshold velocity (0.62 m/s), by over a factor of two, occurs with Class 2. For neutral conditions this yields a threshold wind velocity of 9 and 15 m/s, respectively. Analysis of the ECMWF wind speeds in the region for the period of August 1990 through August 1991 indicated that the 10 m wind speed never exceeded 12 m/s. Therefore only Class 3 dust emissions are considered for the computation. The domain of the emission area is shown in Fig. 4 which also illustrates the percentages (P in Eq. (10)) of each square assigned to Class 3.

3.5. Model calculation procedure

The Hysplit model with the PM_{10} emission algorithm was run for the period of 1 August 1990 through 31 August 1991. The model was configured such that one puff/particle was emitted from each 0.5° emission cell whenever the wind speed in that cell at that time exceeded the threshold wind speed. There were 586 potential emission cells in the region. Typical dust storm events would result in emissions from 50 to 150 cells.

The model's computational limits are the same as the meteorological grid in the horizontal, 10 km for the vertical domain, and all particle-puffs were dropped 48 h after emission. The resolution of the concentration grid was established with a resolution of 0.25° latitude–longitude and 24 h average PM_{10} air concentrations were computed daily from 08:00 UTC as a layer average from the ground to 10 m. In addition, the model computed gravitational particle settling assuming a mean diameter of 3.0 μm with a density of 2.5 g/cm^3.

Part of the computational period (starting May 1991) corresponded with a comprehensive ground-based measurement program (described in the next section). Computations during this period indicated substantial dust emissions. Fig. 5 shows the emission weighted centroid for all emission cells in any 1 h in which at least one cell had non-zero emissions. Although Fig. 4 showed a southeast to northwest alignment of the emission grid, the actual emission locations are much more narrowly defined along the Persian Gulf coast and southern Iraq. This result is consistent with the independent analysis (Section 2.4) of the streaks shown in Fig. 1, illustrating the strong alignment of the aeolian movement.

4. Results

4.1. PM_{10} measurements

As part of the overall environmental sampling and analysis effort to assess the health risk from oil well fires to US troops in the region, sand samples and ambient particulate matter less than 10 μm (PM_{10}) samples were collected on a daily basis and analyzed (HRA, 1991). Sampling began in Kuwait and Saudi Arabia in early May 1991 and continued through December 1991. The model predicted air concentration data are to be used for health assessments in the area occupied by US troops during the Gulf War period prior to the onset of surface-based sampling (August 1990–April 1991).

Samples were collected using high-volume samplers at nine sites as indicated in Table 2 using United States Environmental Protection Agency reference methods for determining PM_{10} and total suspended particulate matter. The PM_{10} sampler utilizes a specially shaped inlet to inertially separate particulate matter less than 10 μm fraction (which is collected on glass-fiber or quartz fiber filter media) and greater than 10 μm fraction (which is discarded). The total suspended particulate matter unit's specified shelter geometry collects particulate matter up to 50 μm. For each particulate matter sample, the air concentration was determined from the total particulate matter mass collected on the filter divided by the integrated air volume sampled. In addition, the particulate matter filters were analyzed for heavy metals and elemental carbon and silica percentages. Computer-controlled scanning electron

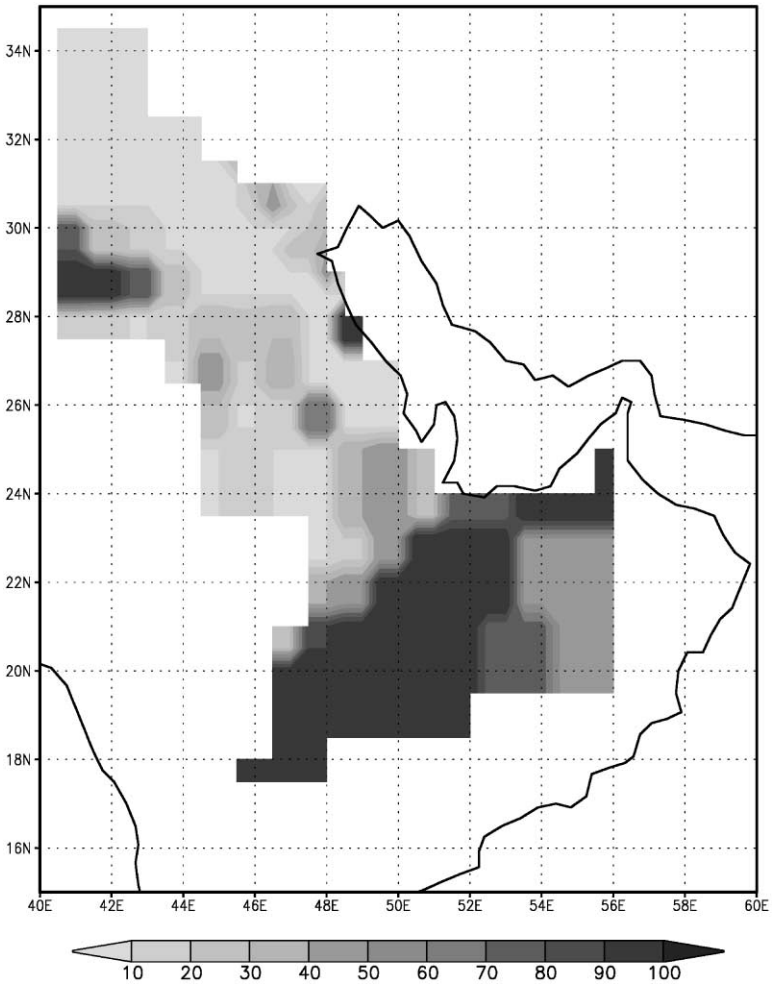

Fig. 4. Percent coverage of active sand sheet and disturbed soils over the potential dust emission domain.

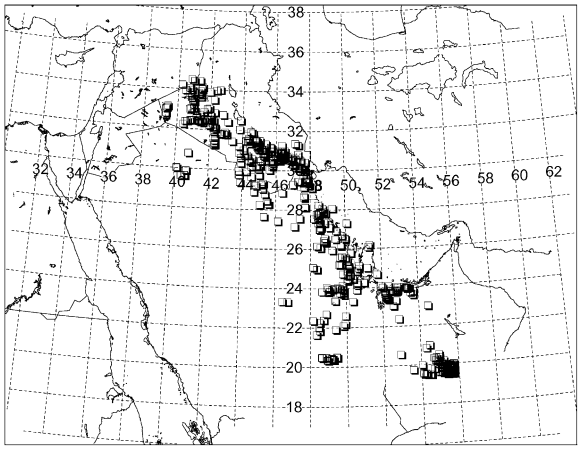

Fig. 5. Centroid of all emission cells for any hour in which at least one cell had non-zero emissions.

microscopy and transmission electron microscopy were used on air and soil samples to determine particle mass distribution and particle type data. Mass distribution results were based on aerodynamic equivalent diameter.

Because the Saudi Arabian samplers were hundreds of kilometers apart while the Kuwaiti samplers were all within a few tens of kilometers of each other, the Camp Thunderock sampler at Doha was used to represent Kuwait. It is just west of the central city and upwind of the urban fugitive emissions. If data at Doha were missing, then the value at the nearest location was used instead. The other sites in order of replacement were the Embassy (19 km), the Military Hospital (27 km), and Ahmadi Hospital (41 km). Cross-correlations of the non-missing concentration measurements between Doha and the other sites were 0.65, 0.81, and 0.58, respectively. Model results are then compared to

Table 2
PM_{10} sampling locations in Kuwait (KU) and Saudi Arabia (SA) in 1991

Site	Name	Location	Period	Coordinates	
1	Khobar Towers	Al-Dhahran, SA	06 May–02 Dec	26.25°N	50.22°E
2	Jubail	Al-Jubayl, SA	08 May–04 Aug	27.07°N	49.53°E
3	King Khalid	Military City, SA	19 May–25 Aug	27.87°N	45.53°E
4	Eskan Village	Ar-Riyadh, SA	25 May–25 Aug	24.55°N	46.85°E
5	Military Hospital	Kuwait City, KU	17 May–02 Dec	29.26°N	48.06°E
6	US Embassy	Kuwait City, KU	19 May–15 Jul	29.38°N	48.00°E
7	Camp Thunderock	Doha, KU	06 Jun–02 Dec	29.37°N	47.80°E
8	Ahmadi Hospital	Al-Ahmadi, KU	06 Jun–06 Jul	29.10°N	48.07°E
9	Camp Abdaly	Abdaly, KU	19 May–05 Jun	30.08°N	47.70°E

measurements at five locations; four in Saudi Arabia and the one composite location representing Kuwait.

During the initial few months of the measurement program there was considerable smoke present due to the oil well fires. Out of all the filter samples collected, 57 of the high-volume samples were analyzed for composition and particle size. The data indicated that mixed clays, silicon-rich and calcium-rich particles accounted for the vast majority of the sample mass in most samples. The PM_{10} material was comprised mainly of sand-based material rather than carbon-chain agglomerates from the oil fires smoke. Aerodynamic equivalent mass distribution results indicated that the majority of the particle mass for most samples occurred in the size ranges less than 10 μm. However, a significant fraction (40%) of the particle mass was observed in the 10–30 μm size range for all samples. These results suggest that we can attribute high PM_{10} measurements to dust storms rather than smoke.

4.2. Calculation versus measurement

The first two months of the sampling contained the largest number of dust events. The model calculations and corresponding measurements at the three coastal locations is shown in Fig. 6 for the period of 16 May through 15 July 1991. A cursory examination shows that during this period measured PM_{10} was frequently in the 100–200 $\mu g/m^3$ range. The model substantially over-predicted concentrations for the large-scale events (predictions > 1000 $\mu g/m^3$) and under-predicted the typical daily average. Considering that there are very few days when the wind velocity exceeds the threshold, it is expected for the model to predict zero most days. Consistent day-after-day low-level measured concentrations (although 100–200 $\mu g/m^3$ may not be considered low in many other regions) are attributed to fugitive emissions, such as vehicular traffic on "dusty" roads and possibly from distant sources, neither of which is part of the model design. Predictions at the two inland stations is shown in Fig. 7. Both measured and modeled concentrations are much lower than along the coast

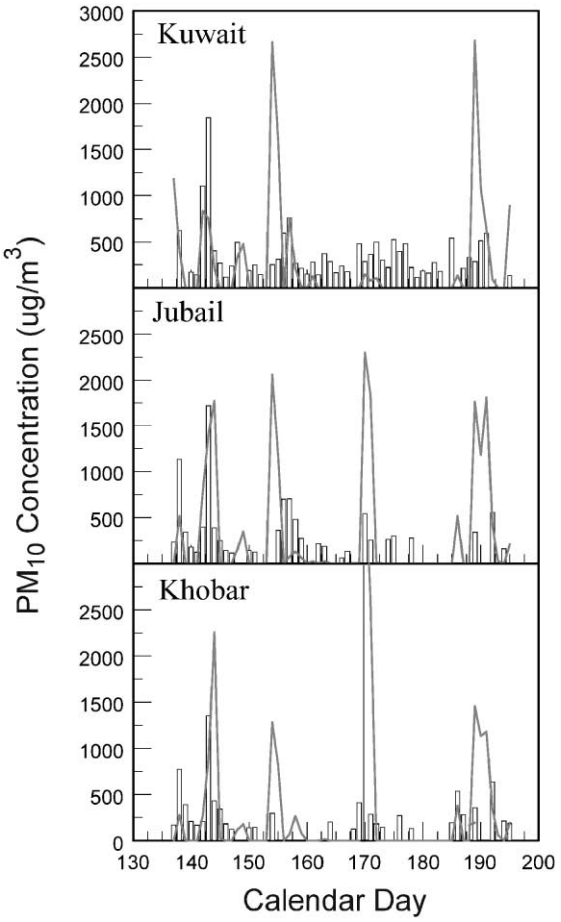

Fig. 6. Measured (vertical bars) and model (solid line) calculated PM_{10} concentrations along the coastal sampling sites from 16 May 1991 through 15 July 1991: Kuwait (top); Jubail (middle); Khobar (bottom). Missing data (which is considerable at some sites) is indicated by a missing bar.

with peaks under 1000 $\mu g/m^3$. These results are consistent with the fact that the strongest winds and hence the greatest dust emissions occurred along the coast (Fig. 5). The predictions and measurements agreed reasonably

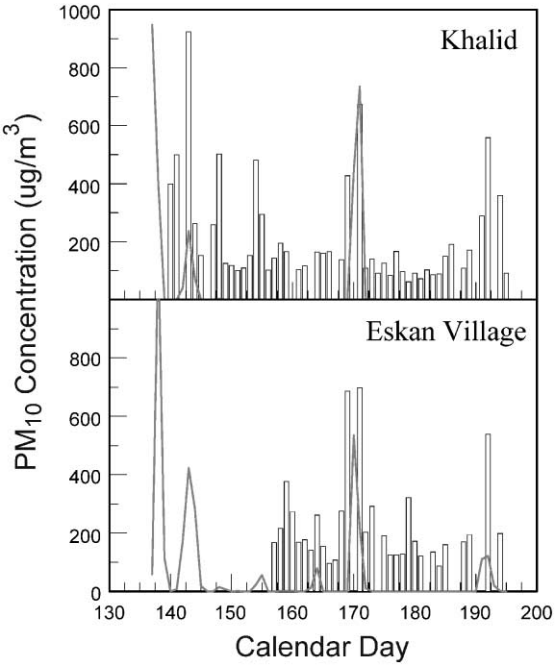

Fig. 7. Measured (vertical bars) and model (solid line) calculated PM_{10} concentrations at the inland sampling stations from 16 May 1991 through 15 July 1991: Khalid (top); Eskan (bottom).

well at the coastal sites for the event on days 143 and 144 and at the inland sites for the event on days 170 and 171.

Another related issue is whether the model can compute the correct number of dust events. Using satellite AVHRR imagery, Walters et al. (1992) documented the number of days for which blowing dust was observed for individual source areas during the period 2 August 1990–31 March 1991. He estimated that there were 44 dusty days over Kuwait in the 235 day period or about 18.7% of the time. The average annual number of days of dust in Kuwait given by Safar (1985) was 10.4% which shows that the number of dusty days was above average at least in Kuwait. One possible explanation for this above average dustiness may be that the surface conditions were significantly disturbed in Kuwait during the period. Counting the number of model computed days with PM_{10} concentrations above zero at the Kuwait sampler for the same period yields 37 days or 15.7%, a result consistent with those of Walters et al. (1992). It does appear that the model is computing about the right number of dust events.

4.3. Model uncertainties

Although there is a tendency toward over-prediction, there is a considerable amount of uncertainty in both the measurement and model prediction. For instance, the linkage between friction velocity and the dust emission flux was derived from the empirical data shown in Fig. 2, which shows a 3-order of magnitude variation in the emission flux for the rather small range of friction velocities. The uncertainty of the model's calculation of PM_{10} air concentration, shown in Figs. 6 and 7, is much smaller that the variability in the emission flux "constant". Some simple sensitivity tests, such as slightly lowering or raising (about 10%) the threshold friction velocity, had tremendous impact upon the calculation by substantially increasing the peak concentrations or virtually eliminating all dust events. The effect was always to cause a significant change in the number of emission cells contributing to an event. This sensitivity suggested that any significant improvement to the model's results required more than an adjustment of the constants developed in Section 2. The large variation in the number of emission cells with changes in threshold friction velocity would be comparable to changing the spatial distribution of the roughness classes. However the manual method by which the model's spatial emission characteristics were derived is not amenable to any simple adjustment.

Another complication is that many of the model calculated peaks are associated with missing measurement data in one or more of the days within or adjacent to the computed dust event. Large-scale dust events (e.g. days 142 and 143) are evident at all the measurement sites and the model's prediction is quite good. Smaller-scale dust events (e.g. days 169–171) are only evident at a few measurement sites and the model prediction is associated with much greater variability. Certainly some of the variability in model performance for the smaller-scale events can be attributed to the spatial variation in the model's parameters. The combination of the uncertainty of the location of low soil threshold regions due to disturbances caused by the war and the rather narrow alignment of emission sources due to strong winds only along the coast (example shown in Fig. 5), all require a more accurate wind direction to correctly align the dust plume with specific sampling locations. A much more difficult task when the dust event is not dominating the region.

4.4. Meteorological factors

There are two model performance issues raised in the previous section that may be related to meteorological factors: the model's over-prediction at the coastal sampling locations and the differences in model performance between large-scale dust events and smaller-scale events. The development of a sea-breeze flow may be a factor in reducing the measured concentrations for the coastal stations due to the inflow of dust-free air. The gridded ECMWF fields would not show such small-scale effects and hence the dust transport calculation would

predict higher concentrations. Predicted concentrations were only overestimated for the coastal samplers.

An examination of the nearby meteorological surface observation sites can provide some information about local wind flows. Meteorological observations collected at locations near the PM_{10} sampling sites archived at the National Climatic Data Center (NCDC, 2000) showed only the coastal station at Dhahran (Site 40416) reporting at regular intervals for May through July of 1991. Kuwait City was mostly missing and the station near Jubail was not available. The Dhahran station is located about 12 km from the sampler at Khobar. Interpretation of differences between EMCWF data and the observation at Dhahran is not conclusive because the observation would have been assimilated into the ECMWF analysis.

The temperature, wind speed and direction are shown for a "no dust" three day period in Fig. 8. Days 133–136 (13–16 May) correspond to the beginning of the sampling and only background PM_{10} levels were reported on those days. The 24 h sampling period runs from local noon (09:00 UTC—vertical dashed line) and the PM_{10} concentration for each day are indicated near the top of the figure. This period is interesting in that it clearly shows the development of a sea-breeze in response to the diurnal heating cycle. Rapidly increasing temperatures in the morning hours peak at local noon with a sudden shift in wind speed and direction from west to northeast. Temperatures then slowly cool in the afternoon before the wind suddenly shifts back to west during the evening hours. The ECMWF 10 m wind directions (not shown) exhibit a comparable shift between the west and northeast directions. Note from Fig. 3 that the coast in that region along the Arabian Gulf runs from northwest to southeast indicating that northeast winds are almost orthogonal to the shoreline.

In contrast the results shown in Fig. 9 are for the large-scale dust event of 21–24 May. The samples collected on day 143 showed the highest concentrations of any day and it is the only day in the period that Dhahran actually reported a dust storm as the current weather observation (between 02:00 and 08:00 UTC). Although there is some indication of a diurnal cycle in speed and temperature, the meteorological data do not suggest the formation of a sea-breeze. The results are interesting in that while the wind speeds are above the typical threshold (9 m/s) for the period of the dust event, the wind direction is from the north, a marginally offshore direction. The surface wind would not be entirely representative of the deeper layer through which the dust is transported and hence a surface wind from the north at Dhahran should not be considered to represent a dust free source region. The ECMWF 10 m winds showed a wind direction of 340° a more inland upwind direction, during the times of the reported dust storm.

The meteorological results are shown in Fig. 10 are for the small scale event of 17–20 June. Although the measurements indicated a dust event in the range of 500–700 $\mu g/m^3$, with the highest values reported at the inland samplers, the model predicted the highest concentrations along the coast, with the peak value at Khobar (Fig. 6). The meteorological data show more of a diurnal cycle than the previous case (Fig. 9) and the

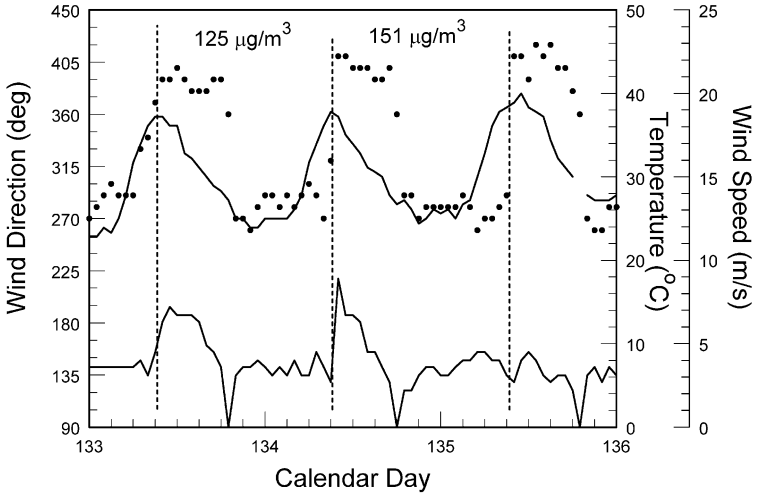

Fig. 8. Summary of hourly surface observations at Dhahran for 13–16 May 1991 (days 133–136) for wind direction (dots), temperature (upper solid line), and wind speed (lower solid line). Local noon (09:00 UTC) is indicated by the vertical dashed line and also represents the approximate collection time of the PM_{10} sample. Air concentrations for the corresponding 24 h sampling period are indicated near the top.

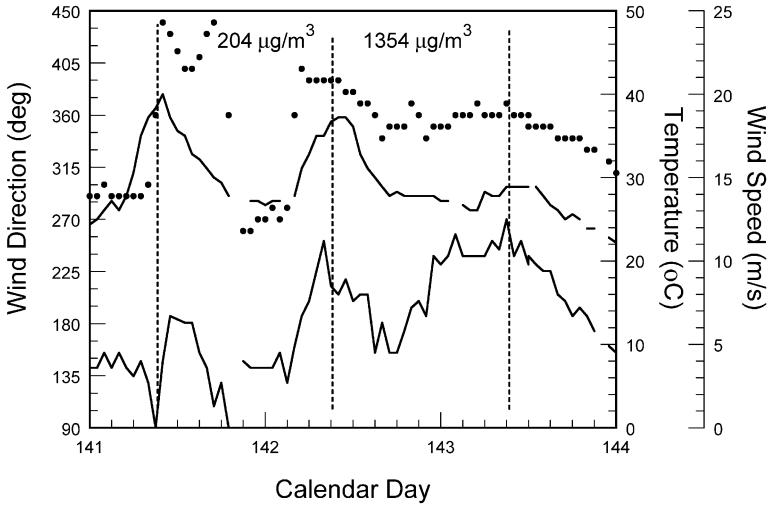

Fig. 9. As in Fig. 8 but for the period 21–24 May 1991 (days 141–144).

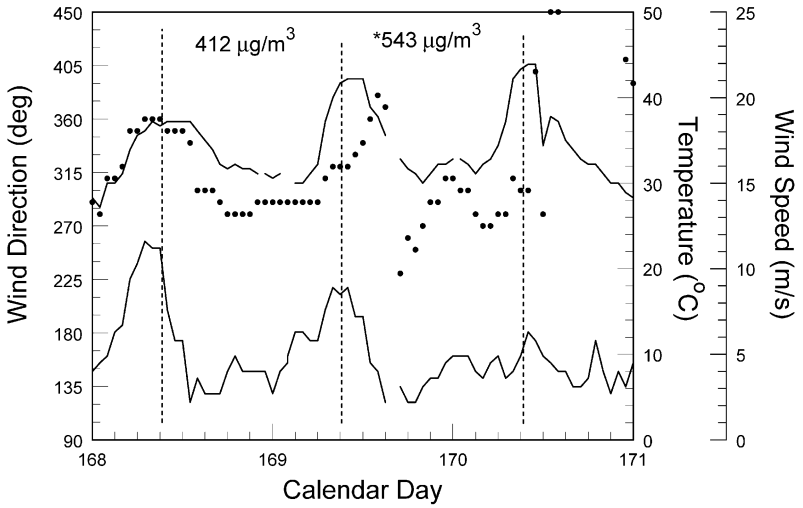

Fig. 10. As in Fig. 8 but for the period 17–20 June 1991 (days 168–171). * Indicates that the Khobar sample was missing that day and the air concentration is taken from the Jubail sampler.

wind direction briefly turns to the northeast (from offshore) followed by a rapid shift to the southwest. Clearly the 24 h collection period represents a range of wind directions where both clean and dust laden air would have contributed to the sample. The ECMWF gridded data only show wind directions from the dust sources to the northwest (290–325°), suggesting a cause for the extreme over-prediction. This case is typical of many of the remaining dust events, where there is much more variability in the model's performance, some evidence for the development of diurnal flow features, and questions about the representativeness of the larger-scale gridded data.

4.5. TOMS aerosol index spatial pattern

It would be informative to compare the spatial pattern of a large-scale dust event with the pattern predicted by the model. One approach is to use the aerosol index (AI—Herman et al., 1997), derived from the Nimbus-7 Total Ozone Mapping Spectrometer (TOMS) instrument. Positive values of AI generally represent

absorbing aerosols (dust and smoke) while negative values represent non-absorbing aerosols. AI has been computed by the NASA TOMS Ozone Processing Team and is available over the Internet (http://toms.gsfc.nasa.gov). The TOMS data can distinguish between different type of aerosol particles based on their size (dust tends to have larger particles than smoke) and absorbing properties in the ultraviolet (Torres et al., 1998). The resolution of each processed data point is 1.0° latitude by 1.25° longitude.

Although one could compare the AI values to the corresponding measurements of PM_{10} air concentrations, unfortunately during the ground-based measurement period that had the greatest number of dust events, the TOMS AI values were dominated by the oil fire's smoke. There was a significant dust event around 4, February 1991, just prior to the start of the fires (smoke was first reported on 9 February and the ground war started on 22 February). The AI image for 4 February as well as the corresponding model prediction for the time step corresponding to the satellite's crossing (about 08:00 UTC) is shown in Fig. 11. For presentation clarity, only AI values greater than 1.0 are shown (0.5 is usually considered to be the noise threshold). The model contour units are in $\mu g/m^3$. Although the densest portion of the AI dust cloud is several hundred kilometers to the north of the model prediction, the overall size and overlap of the patterns is excellent, especially considering the lobes over Kuwait and Oman. Note that the model computed concentrations for a 1000 m layer to produce a closer correspondence to the deeper layer visible to the satellite. In general the satellite instrument is less sensitive to the lower layers in the atmosphere and smaller scale dust events that are

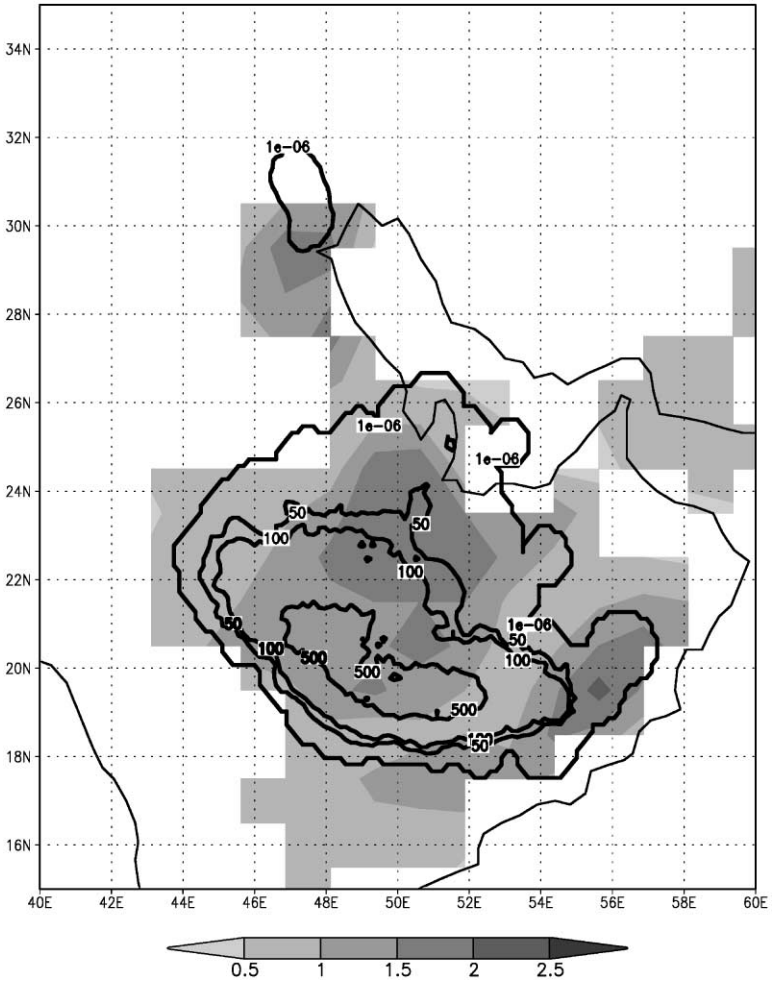

Fig. 11. Aerosol index from the TOMS Nimbus-7 for 4 February 1991 superimposed on model calculated contours of PM_{10} concentration ($\mu g/m^3$) corresponding to the time of the satellite passage.

constrained to a shallow boundary layer may not be detected.

5. Summary and conclusions

A model for the input of PM_{10} dust has been constructed. An assumption of the omnipresence of particles having sizes between 88 and 125 μm was verified by analyses of sampled desert sediments and published data. Threshold friction velocity was modeled to be dependent on surface roughness. Surface roughness in turn was correlated with geomorphology or soil properties. A well tested function related horizontal flux of all aeolian mass to friction velocity and threshold friction velocity. Finally, the ratio of vertical flux of PM_{10} dust to the horizontal flux of all aeolian mass as a function of surface sediment texture was used to express the vertical flux of PM_{10} dust. Textures of all sampled soils were quite close to "sand" texture and consequently only one ratio was used for all soils in the source areas of the area. The model domain is for Kuwait, Iraq, part of Syria, Saudi Arabia, the United Arab Emirates and Oman.

The PM_{10} emission algorithm was incorporated into a Lagrangian transport and dispersion model. Using gridded meteorological data for the region, PM_{10} air concentrations were computed from August 1990 through August 1991. The model predicted about the right number of dust events over Kuwait for the computational period. A more quantitative comparison of model predicted air concentrations with those measured at four locations in Saudi Arabia and one in Kuwait over a 2 month period showed the model to predict each of the major dust storm events but the model consistently over-predicted the PM_{10} air concentrations. The over-prediction at the coastal samplers may be attributed to the development of diurnal flows such as a sea-breeze, features not well represented by the ECMWF data. The results suggest that the model's bias toward over-prediction is due to the entrainment of cleaner air from off-shore. The model performed well for very large-scale dust events where wind speeds consistently exceeded the threshold with little evidence of any small-scale flow features. The measurement data showed that during most days concentrations were in the range of 100–200 $\mu g/m^3$, a feature attributed to fugitive emissions and not predicted by the model's strong wind dependent emission algorithm.

A comparison of the model predicted PM_{10} spatial pattern with the TOMS satellite aerosol index yielded a spatial pattern covering a major portion of Saudi Arabia that was strikingly similar to the measurements. The study demonstrated that it is possible to incorporate an inventory of complex soil characteristics and meteorological data through a modeling approach to produce reasonable estimates of dust storm frequency and their spatial extent.

Acknowledgements

Professor Andrew Warren of the Department of Geography, University College London, was very helpful in providing bibliographic material.

References

Binda, P.L., 1983. On the skewness of some aeolian sands from Saudi Arabia. In: Brookfield, M.E., Ahlbrandt, T.S. (Eds.), Eolian Sediments and Processes, Developments in Sedimentology, vol. 38. Elsevier, Amsterdam, pp. 27–39.

Buringh, P., 1960. Soils and soil conditions in Iraq. Director General of Agricultural Research, Baghdad, 322pp.

Draxler, R.R., 1992. Hybrid single-particle Lagrangian integrated trajectories (HY-SPLIT): Version 3.0—User's guide and model description. NOAA Tech. Memo. ERL ARL-195, 26pp. and Appendices.

Draxler, R.R., 1996. Trajectory optimization for balloon flight planning. Weather and Forecasting 11, 111–114.

Draxler, R.R., Hess, G.D., 1997. Description of the HYSPLIT_4 Modeling System. NOAA Tech. Memo. ERL ARL-224, December, 24pp.

Draxler, R.R., Hess, G.D., 1998. An overview of the HYSPLIT_4 modelling system for trajectories, dispersion, and deposition. Australian Meteorological Magazine 47, 295–308.

ECMWF 1995. The description of the ECMWF/WCRP level III-a global atmospheric data archive. European Centre for Medium-Range Weather Forecasts, Reading, Berkshire, England.

El-Baz, F., 1994. Gulf war disruption of the desert surface in Kuwait. In: El-Baz, F., Makharita, R.M. (Eds.), The Gulf War and the Environment. Gordon and Breach Science Publishers, US, 206pp, pp.131–161.

Gharib, I., Foda, M., Al-Hashash, M., Marzouk, F., 1985. A study of control measures of mobile sand problems in Kuwait air bases. Kuwait Institute for Scientific Research, Report No. KISR 1696, Safat, Kuwait.

Gillette, D., Adams, J., Muhs, D., Kihl, R., 1982. Threshold friction velocities and rupture moduli for crusted desert soil for the input of soil particles into the air. Journal of Geophysical Research 87, 9003–9015.

Gillette, D., Herbert, G., Stockton, P., Owen, P., 1996. Causes of the fetch effect in wind erosion. Earth Surface Processes and Landforms 21, 641–659.

Gillette, D.A., 1983. Threshold velocities for wind erosion on natural terrestrial arid surfaces (a summary). In: Pruppacher, H., Semonin, R., Slinn, W. (Eds.), Precipitation Scavenging, Dry Deposition, and Resuspension. Vol 2, Elsevier, New York, pp. 1047–1057.

Gillette, D.A., Adams, J., Endo, A., Smith, D., 1980. Threshold velocities for input of soil particles into the air by desert soils. Journal of Geophysical Research 85, 5621–5630.

Gillette, D.A., Fryrear, D.W., Gill, T.E., Ley, T., Cahill, T.A., Gearhart, E.A., 1997. Relation of vertical flux of PM_{10} to

total aeolian horizontal mass flux at Owens Lake. Journal of Geophysical Research 102, 26009–26015.

Gillette, D.A., Marticorena, B., Bergametti, G., 1998. Changing the roughness length by saltating grains: experimental assessment, test of theory and operational parameterization. Journal of Geophysical Research 103, 6203–6209.

Greeley, R. and Iversen, J.D., 1985. Wind as a Geological Process on Earth, Mars, Venus and Titan. Cambridge University Press, Cambridge, 333pp.

Herman, J.R., Bhartia, P.K., Torres, O., Hsu, C., Seftor, C., Celarier, E., 1997. Global Distribution of UV-Absorbing Aerosols From Nimbus-7/TOMS Data. Journal of Geophysical Research 102, 16911–16922.

HRA, Kuwait Oil Fire Health Risk Assessment, 1991. Final Report No. 39-26-L192-91, Appendix G, Sand and Ambient Air Sample Analysis, Vol I. US Army Environmental Hygiene Agency, Aberdeen Proving Ground, MD 21010.

Hurley, P., 1994. PARTPUFF—A Lagrangian particle–puff approach for plume dispersion modeling applications. Journal of Applied Meteorology 33, 285–294.

Iversen, J.D., White, B.R., 1982. Saltation threshold on Earth, Mars and Venus. Sedimentology 29, 111–119.

Karyampudi, V.M., Palm, S.P., Reagen, J.A., Fang, H., Grant, W.B., Hoff, R.M., Moulin, C., Pierce, H.F., Torres, O., Browell, E.V., Melfi, S.H., 1999. Validation of the Saharan dust plume conceptual model using Lidar, Meteosat, and ECMWF Data. Bulletin of the American Meteorological Society 6, 1045–1075.

Li, L., Martz, L.W., 1994. System of numeric models for sand particle transport by wind. Journal of Geophysical Research 99, 12999–13012.

Marticorena, B., Bergametti, G., 1995. Modeling the atmospheric dust cycle, 1, Design of an a soil-derived dust emission scheme. Journal of Geophysical Research 100, 16415–16430.

Marticorena, B., Bergametti, G., Gillette, D., Belnap, J., 1997. Factors controlling threshold friction velocity in semiarid and arid areas of the United States. Journal of Geophysical Research 102, 23277–23287.

McKenna-Neuman, C., Nickling, W.G., 1994. Momentum extraction with saltation: Implications for experimental evaluation of wind profile parameters. Boundary-Layer Meteorology 68, 35–50.

National Climatic Data Center (NCDC), 2000. Surface data, hourly and three hourly—TD9956, DATSAV3, Asheville, NC.

Safar, M., 1985. Dust and duststorms in Kuwait. Meteorological Department of the Directorate General of Civil Aviation, Kuwait.

Skocek, V., Saadallah, A., 1972. Grain size distribution, carbonate content and heavy minerals in aeolian sands, Southern Desert, Iraq. Sedimentary Geology 8, 29–46.

Stevens, J., 1978. Post pluval changes in the soils of the Arabian Peninsula. In: Brice, W. (Ed.), The Environmental History of the Near and Middle East Since the Last Ice Age. Academic Press, London, pp. 384 pp. 263–274.

Torres, O., Bhartia, P.K., Herman, J.R., Ahmad, Z., Gleason, J., 1998. Derivation of aerosol properties from satellite measurements of backscattered ultraviolet radiation: theoretical basis. Journal of Geophysical Research 103, 17099–17110.

United Kingdom Series Edition 5211 2-GSGS, 1980. (Revision of the U.S. Geological Survey and Arabian-American Oil Company, compiler, U.S. Geological Survey Misc. Geol. Inv. Map I-270) Geological Map of the Arabian Penninsula scale 1 : 2,250,000.

Walters, K., Traxler, K., Gilford, M., Arnold, R., Bonam, R., Gibson, K., 1992. Gulf war weather. USAF ETAC/TN-92/003, USAF Environmental Technical Applications Center, Scott Air Force Base, IL 6222, -5438, 245pp.

Westphal, D.L., Toon, O.B., Carlson, T.N., 1987. A two-dimensional numerical investigation of the dynamics and microphysics of Saharan dust storms. Journal of Geophysical Research 92, 3027–3029.